CHAPTER 4

Synthesis of polymer stabilised Fe^0 and Fe/Ni bimetallic nanoparticles for the removal of Cr(VI) and triphenylmethane dyes from water

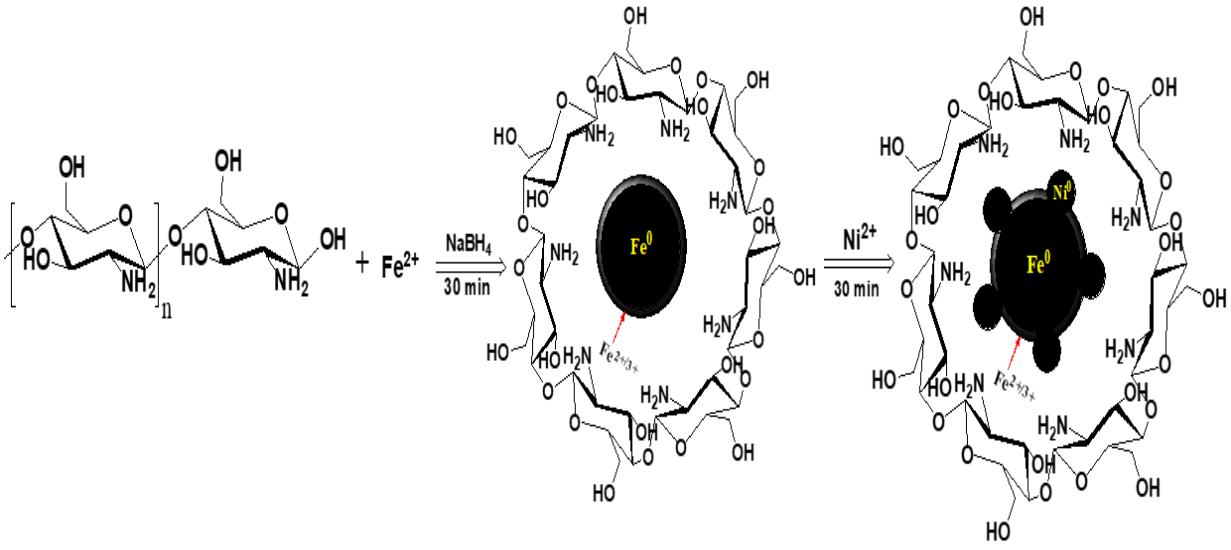

Chitosan CS-Fe CS-Fe/Ni

Chapter 4

Synthesis of polymer stabilised Fe^0 and Fe/Ni bimetallic nanoparticles for the removal of Cr(VI) and triphenylmethane dyes from water

4.1. Introduction

The zero valent iron (Fe^0) nanoparticles are considered a potential green material to remediate wastewater due to the availability of iron as recycled material and its capacity to degrade some contaminants completely. Even though Fe^0 nanoparticles show high reactivity towards pollutants, their major limitations are reactivity loss with time due to the precipitation of iron oxides on the surface of Fe^0 and their agglomeration tendency due to magnetic properties[1,2]. The addition of a second metal to the Fe^0 enhances the properties of zero valent iron through the synergetic effect of two distinct metals, which serves as a protective agent against corrosion of the iron surface. Till now, different iron-based bimetallic nanoparticles such as Fe/Al, Fe/Pd, Fe/Ni, Fe/Cu, Fe/Zn, Fe/Ag, Fe/Au, Fe/Co and Fe/Pt were synthesised and their catalytic elimination properties were studied in various pollutants[3,4]. Cost-effectiveness, efficiency, and toxic effect of second metal should be considered the three important criteria for selecting second metal regarding water pollution remediation. Among the synthesised bimetallic nanoparticles, Fe/Ni nanoparticles have special consideration because of their ability to enhance the formation of atomic hydrogen on the surface of Fe^0 and their ability to improve electron transfer between nanoparticles and pollutants. In addition, catalytic metal Ni is less toxic and economically feasible than other catalytic metals[5–8].

Although Fe^0 and Fe/Ni nanoparticles get considerable attention due to their high specific surface area and small size, the Fe^0 nanoparticles are highly reactive towards air and water. To develop the Fe^0 and Fe/Ni nanoparticles as an efficient remediating agent, they could be modified or combined with different methods. These methods are mostly immobilising Fe0 nanoparticles onto supports like zeolite, polymers, etc., and combining Fe^0 nanoparticles with other techniques like sonication and UV irradiation[9]. Even though the stabilisation of Fe^0 is extensively studied, further investigation is needed for the stabilisation of Fe^0 and Fe/Ni nanoparticles due to their potential capacity for water contaminant degradation and small footprint. This study incorporates chitosan, a

biopolymer, with Fe^0 and Fe/Ni nanoparticles. Only limited studies have presently been reported on the stabilisation of Fe^0 nanoparticles by chitosan. Chitosan is a biopolymer produced by the deacetylation of chitin, derived from the exoskeleton of crustaceans and cartilages of molluscs. The presence of free amino and hydroxyl groups in chitosan makes them material with high adsorption potential and multipurpose materials in industrial applications. The other favourable characteristics of chitosan as an adsorbent are its macromolecular structure, non-toxicity, biocompatibility, biodegradability, low cost, etc.[10,11]. Previous studies of chitosan as a stabilising agent showed that it produces stabilised metallic (silver, gold, iron and platinum) nanoparticles with moderately average diameters[12,13].

In this work, we have synthesised chitosan-stabilised Fe^0 (CS-Fe) and chitosan-stabilised Fe/Ni (CS-Fe/Ni) nanoparticles by using chitosan as a stabilising agent for the removal of hexavalent chromium (Cr(VI)) and triphenylmethane dyes (malachite green and methyl blue). The properties of malachite green and methyl blue dyes have been discussed in chapter 3. We have investigated the influence of different parameters, such as the initial pollutant concentration, dosage of nanoparticles, contact time and pH of the solution in pollutant removal. We have also studied the effect of ionic strength of the solution in the removal of triphenylmethane dyes. Figure 4.1 represents malachite green (A) and methyl blue (B) chemical structure.

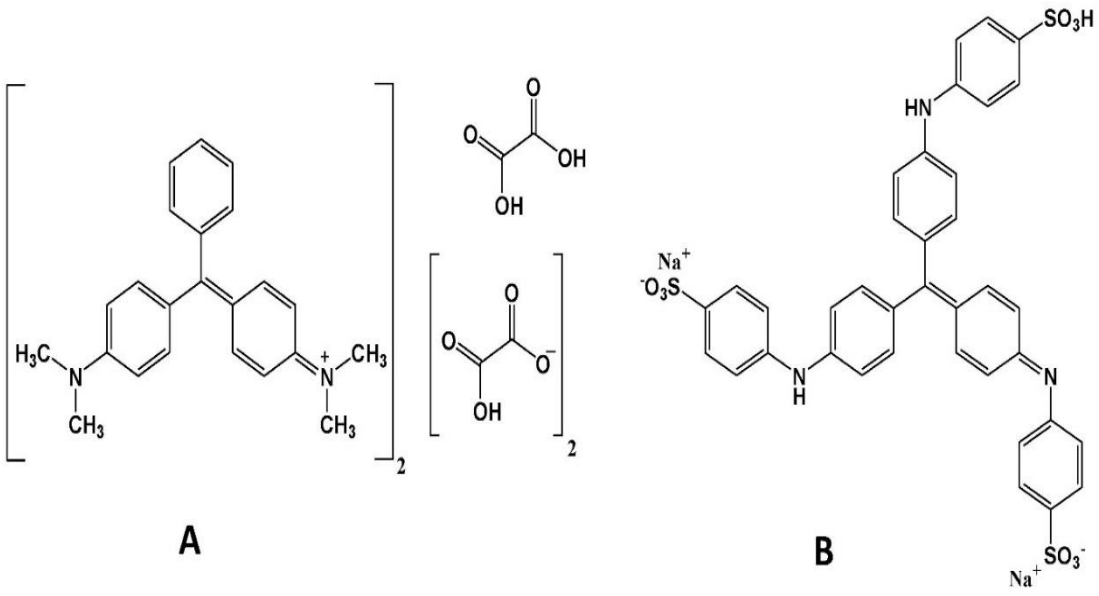

Figure 4.1 *Chemical structure of Malachite Green (A) and Methyl Blue (B)*

4.2. Experimental details

4.2.1 Synthesis of CS-Fe and CS-Fe/Ni nanoparticles

CS-Fe and CS-Fe/Ni nanoparticles were prepared using sodium borohydride as reducing agent[14,15]. Chitosan (0.5 %), the stabiliser used to synthesise CS-Fe and CS-Fe/Ni nanoparticles, was dissolved in dilute acetic acid using ultrasonication. $FeCl_3.6H_2O$ (0.973 g) was prepared in 50 mL deionised water to synthesise CS-Fe nanoparticles. The prepared $FeCl_3.6H_2O$ solution was incorporated with the dissolved chitosan solution in a round bottom flask under the nitrogen atmosphere. The mixture was stirred for 15 minutes using a magnetic stirrer and 50 mL of $NaBH_4$ (0.544 g) solution prepared in an ethanol-water system was added drop by drop into this mixture and stirred vigorously and continuously for 30 minutes. The formation of the black coloured precipitate indicates the presence of CS-Fe. The formation reaction of CS-Fe is represented in equation (4.1).

$$CS + Fe^{2+} + 2BH_4^- + 6H_2O \rightarrow CS - Fe^0 + 2B(OH)_3 + 7H_2O \qquad (4.1)$$

The method for synthesis of CS-Fe/Ni nanonoparticles was similar to that of chitosan stabilised Fe nanoparticles, except that the $NiSO_4.6H_2O$ solution was added to the prepared nanoparticles. $NiSO_4.6H_2O$ (0.089 g) solution was prepared in 10 mL deionised water added to freshly prepared CS-Fe solution and agitated for another 30 minutes. This would lead to the formation of CS-Fe/Ni nanoparticles depicted by equation (4.2). The prepared nanoparticles were collected through vacuum filtration and the nanoparticles were rinsed with deionised water, absolute ethanol and acetone successively. The prepared nanoparticles were lyophilised and stored in a sealed bottle.

$$CS - Fe_x^0 + yNi^{2+} \rightarrow CS - Fe_{x-y}^0 Ni^0 + Fe^{2+} \qquad (4.2)$$

4.2.2 Batch experiments

Cr(VI) removal studies

The details of batch experiments followed for Cr(VI) removal were discussed in chapter 2. Different parameters examined in this study for Cr(VI) removal were nanoparticle dosage (1-5 g/L), initial concentration of Cr(VI) (1-7 mg/L), initial pH of the solution (3-9) and contact time (15-60 min). The pH of the solution has been adjusted using 1.0 M NaOH and 1.0 M H_2SO_4. All experiments were performed with a duplicate.

Dye removal studies

The method followed for the batch experiments of dye removal were already given in chapter 3. Various parameters investigated in the present study are nanoparticle dosage (0.5-2 g/L), initial concentration of dye (50-150 mg/L), initial pH of the solution (4-12), contact time (60-180 min) and ionic strength of the solution (0.001-0.1 M). To study the influence of ionic strength, 20 mL of NaCl solution was added to 40 mL of 50 mg/L dye solution and the concentration of the NaCl was varied from 0.001 M to 0.1 M. The samples were analysed for the residual dye concentration using a UV-visible spectrophotometer and the experiments were performed with a duplicate.

4.2.3 Characterisation and analytical techniques used

The prepared nanoparticles were lyophilised using Operon FDU 7003 lyophiliser. The particle size and morphology of the CS-Fe and CS-Fe/Ni nanoparticles were analysed using HRTEM, XPS and FTIR. Details of characterisation techniques are discussed in chapter 2. In this case, the FTIR spectra of CS, CS-Fe and CS-Fe/Ni nanoparticles before and after the reaction with dyes were investigated through Fourier transform infrared spectrometer (SHIMADZU IR Affinity-1) in the wavelength range of 4000 – 600 cm^{-1}. Samples for FTIR analysis were prepared by mixing KBr with the samples and pressed into small thin pellets. The degradation products of MG dye using CS-Fe/Ni nanoparticles was analysed by GC-MS/MS and the procedure followed for GC-MS/MS analysis was discussed in chapter 3.

4.3. Results and discussion

4.3.1 Characterisation of CS, CS-Fe and CS-Fe/Ni nanoparticles

HRTEM

The transmission electron micrographs of the CS-Fe/Ni and CS-Fe, as shown in figure 4.2, revealed that a layer of grey material covered the spherical metallic nanoparticle. This indicates the core-shell structure of the nanoparticle. As chitosan was used as a stabiliser, it was concluded that the Fe^0 nanoparticle would have been coated with a layer of chitosan as the shell. By randomly counting around 50 nanoparticles in the HRTEM photograph, the CS-Fe and CS-Fe/Ni nanoparticles' average diameter was estimated as 14.87 nm and 9.2 nm respectively, with a metallic core of 9.73 nm and 5.57 nm. It is believed that the chitosan reduced the agglomeration tendency of nanoparticles that arose from the magnetic

property of iron nanoparticles and protects the iron nanoparticle from oxidation by binding Fe^0 with hydroxyl and amine groups of the chitosan[16].

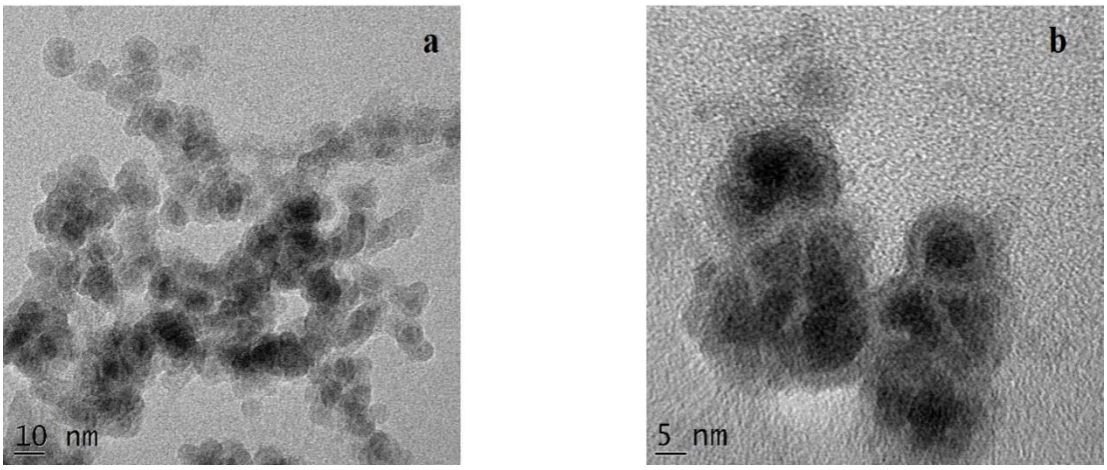

Figure 4.2 *HRTEM image of (a) CS-Fe/Ni and (b) CS-Fe nanoparticles*

XPS

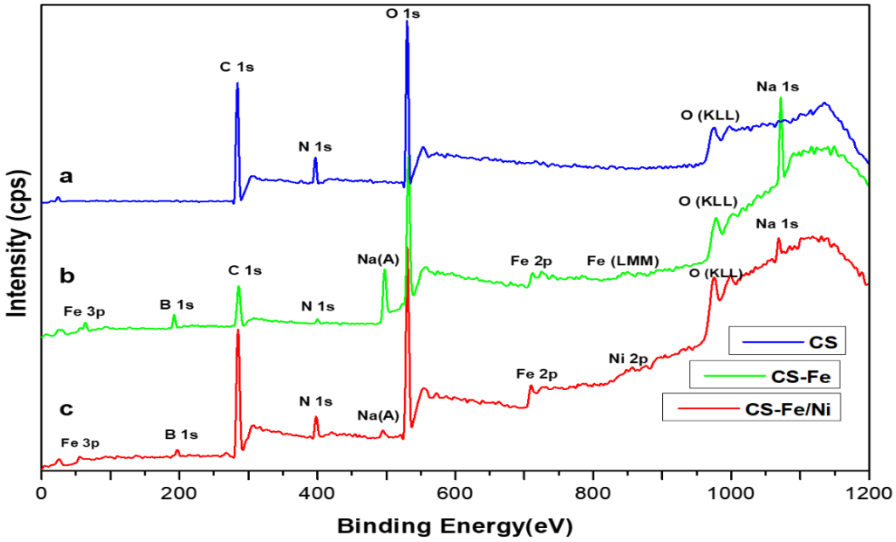

Figure 4.3 *XPS wide scan survey of (a) CS (b) CS-Fe and (c) CS-Fe/Ni nanoparticles*

The composition of the nanoparticles and oxidation states of elements in the nanoparticles were analysed by X-ray photoelectron spectroscopy (XPS). Being a surface analysing technique, XPS can investigate only up to 5-10 nm depth of the sample[17]. XPS wide scan spectra of CS, CS-Fe and CS-Fe/Ni are shown in Figure 4.3. From these spectra, it was evident that C, N, O, Fe and Ni were mainly present in CS-Fe/Ni nanoparticles. They also contained small amounts of elements B and Na, which were the reaction residues from

the preparation of nanoparticles. Compared with the parent CS, the main difference between CS-Fe/Ni and CS-Fe were the emergence of peaks corresponding to the binding energy of Fe and Ni in CS-Fe/Ni and that of Fe in CS-Fe nanoparticles. Even though N 1s was more predominant in CS, a decrease in intensity of N 1s was observed for CS-Fe and CS-Fe/Ni and this may be due to the complexation of N 1s with iron nanoparticles.

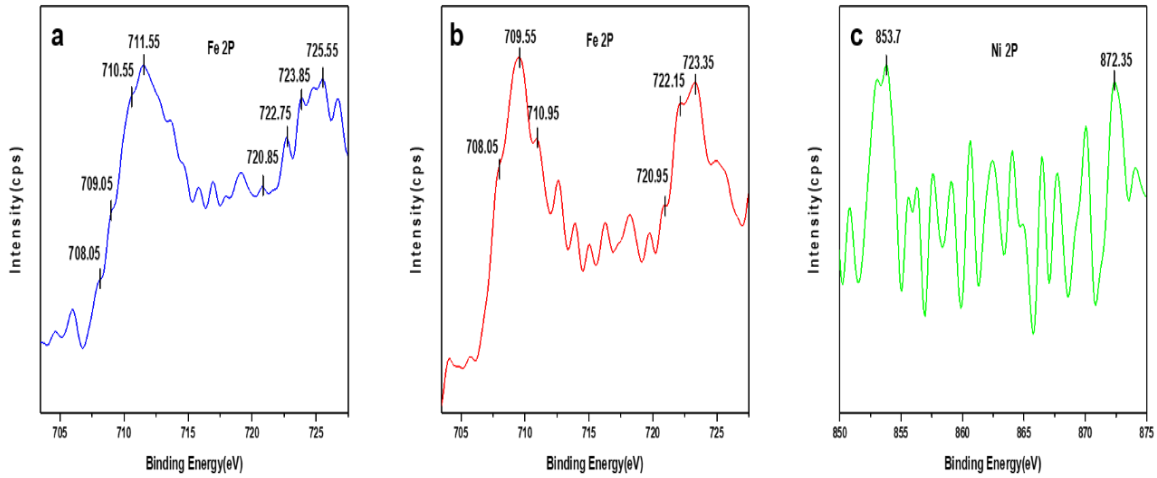

Figure 4.4 *Detailed XPS spectra of (a) Fe 2P in CS-Fe (b) Fe 2p and (c) Ni 2P in CS-Fe/Ni nanoparticles*

A comparison of Fe 2P spectra of CS-Fe and CS-Fe/Ni nanoparticles and Ni 2P spectra of CS-Fe/Ni nanoparticles are shown in figure 4.4. The existence of zero valent iron was confirmed by peaks at around 708.05 eV and 720.95 eV, which corresponds to the $2p^{3/2}$ and $2p^{1/2}$ binding energies of Fe^0 in CS-Fe/Ni nanoparticles[18,19]. The predominant photoelectron peak of CS-Fe/Ni at 709.55 eV and 722.15 eV matched with the binding energies of $2p^{3/2}$ and $2p^{1/2}$ of Fe^{2+} in FeO[20]. The results revealed that the CS-Fe/Ni nanoparticles were covered with a thin iron oxide shell, mainly FeO. The detailed Fe 2P spectrum on the CS-Fe nanoparticles mainly consists of Fe^{3+} species, indicated by the major peak around 711.55 eV and 725.55 eV, which belonged to the binding energies of $2p^{3/2}$ and $2p^{1/2}$ of Fe^{3+} respectively[16]. Compared with the CS-Fe/Ni, the intensity of peaks around 708.05 eV and 720.85 eV was less in CS-Fe, which indicated that more metallic iron was oxidised in CS-Fe. The Fe^{3+} species in samples may be due to the presence of FeO(OH), Fe_3O_4, Fe_2O_3 or Fe^{3+}–chitosan complex. The oxidation of iron that occurred during the detection process might have resulted in the high intensity of the Fe^{3+} peaks in the samples. The Ni 2P detailed spectra in CS-Fe/Ni was complex due to the interaction between iron and chitosan. The peak at 853.7 eV and 872.35 eV corresponds

to the $2p^{3/2}$ and $2p^{1/2}$ binding energies of Ni^{2+} respectively in CS-Fe/Ni nanoparticles[21]. This may be due to the oxidation of Ni on the surface of Fe^0.

4.3.2 Cr(VI) removal studies

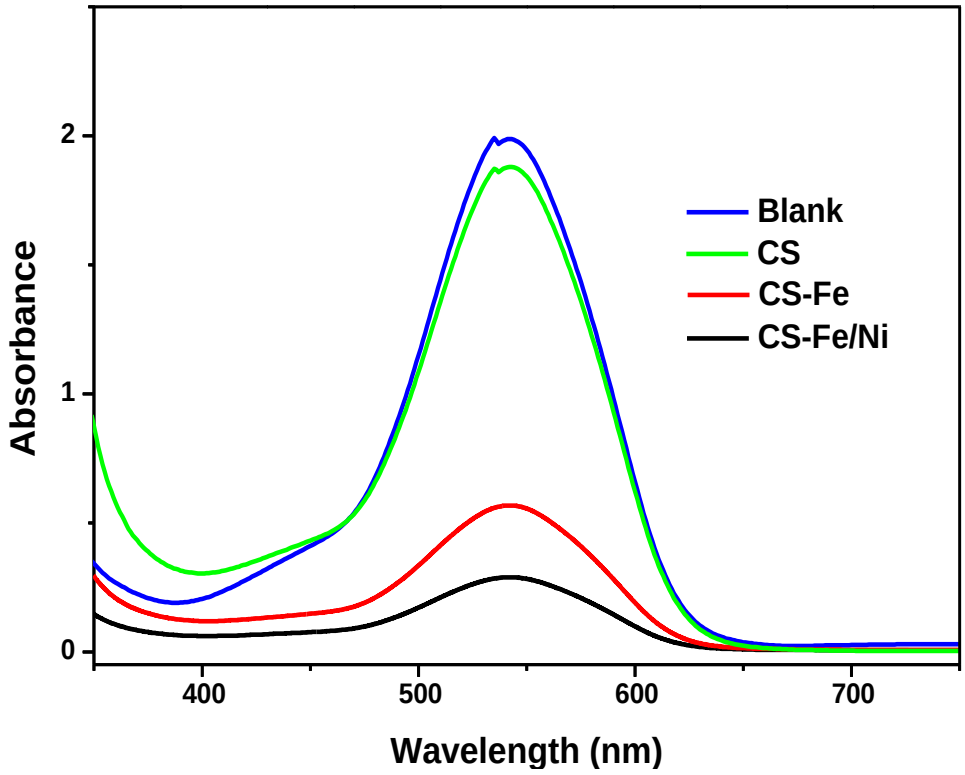

Figure 4.5 *UV-visible spectra of Cr(VI) after treating CS, CS-Fe and CS-Fe/Ni nanoparticles*

Figure 4.5 shows the UV-visible spectra of Cr(VI) treated using CS, CS-Fe and CS-Fe/Ni nanoparticles. The results show that the highest removal efficiency was exhibited by CS-Fe/Ni nanoparticles, followed by CS-Fe nanoparticles and the lowest by chitosan. The high removal efficiency could be due to the small particle size of the CS-Fe/Ni nanoparticles since chitosan on the surface of the nanoparticles causes the electrostatic or steric repulsion, thereby preventing the aggregation of the nanoparticles[22]. In addition to this, previous studies indicate that chitosan has a high tendency to chelate with Fe^{3+} using free amino groups and hydroxyl groups present in them, inhibiting the Fe^{3+}- Cr^{3+} precipitation on the surface of CS-Fe/Ni nanoparticles. It is important since the formation of Fe^{3+}- Cr^{3+} oxide/hydroxide precipitates can inhibit the electron transfer from Fe^0 to Cr(VI), thereby decreasing the Cr(VI) removal efficiency[23]. The better removal efficiency of CS-Fe/Ni nanoparticles compared to CS-Fe nanoparticles could be due to the galvanic effect of Ni. These results match with our previous assumption discussed in chapter 3. Bimetallisation

of Fe^0 nanoparticles improves iron-based nanoparticles' reactivity through better electron transfer via catalytic metal Ni. In the same way, chitosan stabilised bimetallic Fe/Ni nanoparticles have superior removal efficiency than chitosan stabilised Fe nanoparticles. The amino and hydroxyl functional groups present in the chitosan itself show little Cr(VI) removal efficiency through adsorption via electrostatic attraction[24].

Effect of the nanoparticle dosage

Figure 4.6a shows the effect of nanoparticle dosage on the removal of Cr(VI) using CS, CS-Fe and CS-Fe/Ni nanoparticles by keeping the initial concentration of Cr(VI) (5 mg/L) and contact time (30 min) as constant. The nanoparticle dosage varies from 1 to 5 g/L. CS-Fe/Ni nanoparticles showed 95 % removal efficiency at a dosage of 5 g/L of the nanoparticle. However, CS-Fe and chitosan show only 81 % and 25 % removal efficiency at the same dosage. As the dosage of nanoparticles increases, the availability of active surface area and reactive sites also increases and more Cr(VI) removal occurs.

Effect of the initial concentration of Cr(VI)

As discussed previously, a fixed quantity of nanoparticles only removes a specific amount of Cr(VI). This study also shows a similar increase in Cr(VI) removal efficiency when the initial Cr(VI) concentration diminishes from 7 mg/L to 1 mg/L. The nanoparticle dosage (4 g/L) and contact time (30 minutes) were kept constant. Figure 4.6b shows the effect of the initial concentration of Cr(VI) in removing Cr(VI) using prepared nanoparticles, maintaining all other parameters as constant. The highest removal efficiency was observed in 1 mg/L Cr(VI) solution and the lowest removal efficiency in 7 mg/L Cr(VI) solution. The decreasing order of Cr(VI) removal efficiency by nanoparticle were CS-Fe/Ni > CS-Fe > CS. The formation of Fe^{3+}-Cr^{3+}precipitate on the surface of nanoparticles suppresses further reduction of Cr(VI). In higher Cr(VI) concentration, Fe^{3+}- Cr^{3+}precipitate was formed more fastly than lower Cr(VI) concentration.

Effect of contact time

Figure 4.6c displays the effect of contact time on the removal of Cr(VI) using prepared nanoparticles. CS does not show significant removal efficiency after 30 minutes. However, in the case of CS-Fe and CS-Fe/Ni nanoparticles, they are active upto 45 minutes and after that there is drastic reduction in the removal efficiency and reaches a plateau. Cr(VI) removal efficiency of CS, CS-Fe and CS-Fe/Ni nanoparticle were 17 %, 92 % and 93 %

respectively at 45 minutes. With the increase in contact time, the pH of the solution increases due to the reactive removal utilisation of H^+ ions during iron corrosion. This also causes a drop in the Cr(VI) removal.

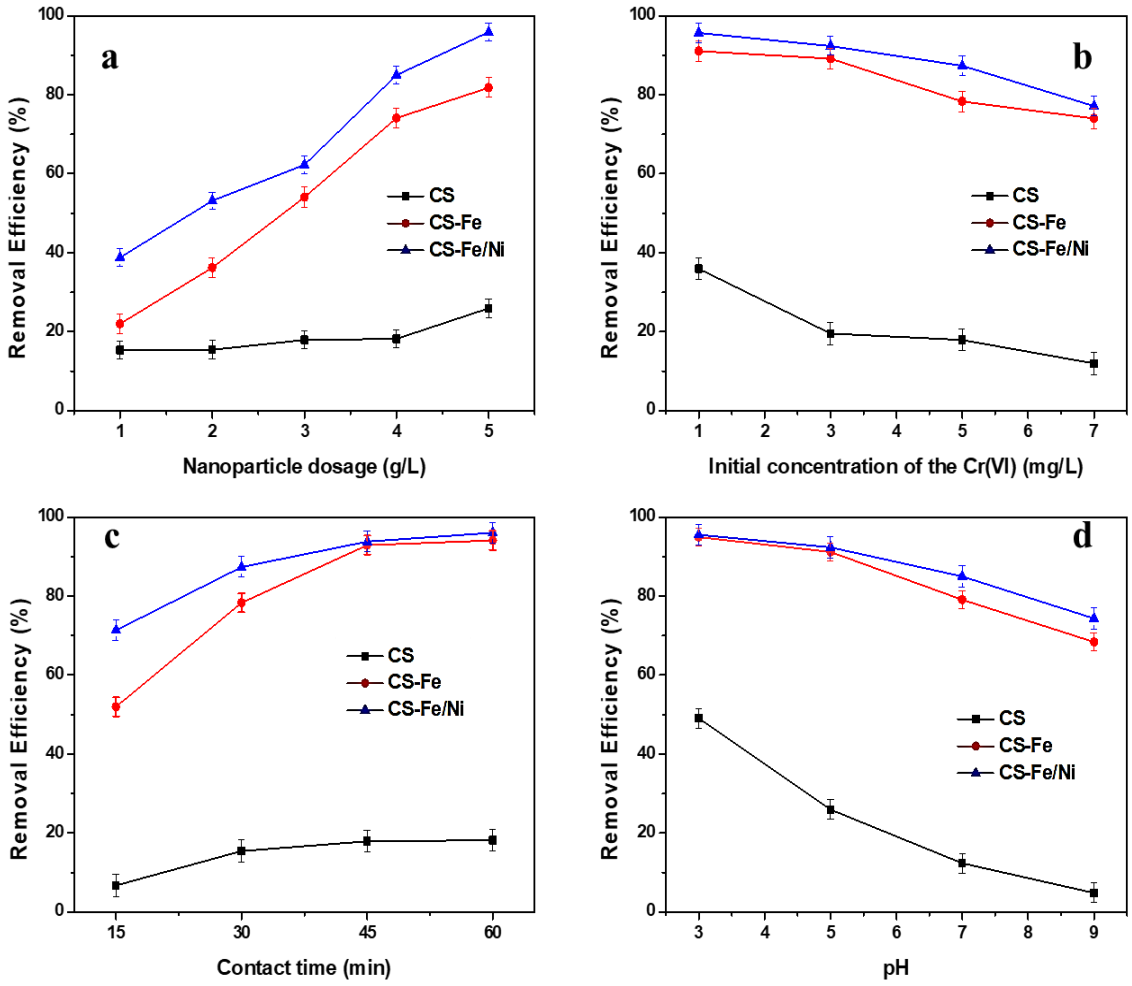

Figure 4.6 *(a) Effect of nanoparticle dosage,(b)Effect of initial concentration of Cr(VI), (c) Effect of contact time and (d) Effect of pH in Cr(VI) removal using CS, CS-Fe and CS-Fe/Ni nanoparticles*

Effect of pH

The effect of pH on removing Cr(VI) (figure 4.6d) was studied using prepared nanoparticles while keeping nanoparticle dosage (4 g/L), initial Cr(VI) concentration (5 mg/L) and contact time were kept constant. The results show that the lower pH of the solution has better removal efficiency than the higher pH. Interestingly, CS exhibits 49 % removal efficiency at pH 3, which may be due to the electrostatic attraction between positively charged chitosan (due to the protonation of amino groups) and Cr(VI)

oxyanions. With the increase in pH of the solution, electrostatic repulsion occurs due to OH^- ions and decreases the Cr(VI) removal efficiency. In this case, CS-Fe/Ni nanoparticles obtained the highest removal efficiency compared to CS and CS-Fe nanoparticles. Even in CS-Fe and CS-Fe/Ni nanoparticles, more removal efficiency was obtained at lower solution pH. Coupled with adsorptive elimination by chitosan, the destruction of iron oxide shell at lower pH also played a critical role in Cr(VI) removal.

4.3.3 Dye removal studies

UV-visible spectroscopy

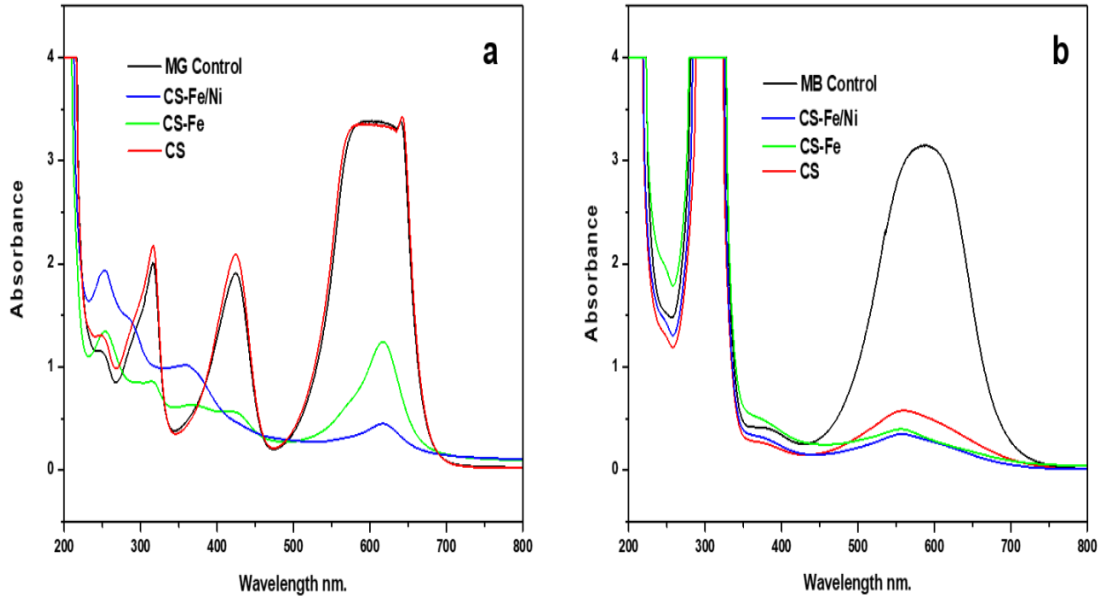

Figure 4.7 *UV-Visible spectra of (a) MG and (b) MB dye removal using CS, CS-Fe and CS-Fe/Ni nanoparticles*

The MG and MB dye removal efficiency were studied using CS, CS-Fe and CS-Fe/Ni nanoparticles through UV-visible spectroscopy as shown in figure 4.7. The disappearance of MG characteristic peaks and emergence of new peaks after adding CS-Fe and CS-Fe/Ni nanoparticles indicate that MG removal was through degradation and adsorption, which is matched with our previous assumption discussed in chapter 3. Dye solution containing CS-Fe and CS-Fe/Ni nanoparticles show high removal efficiency within 60 minutes and the chitosan does not significantly influence the degradation of MG[29]. For the removal of MB, the CS, CS-Fe and CS-Fe/Ni nanoparticles showed high dye decolourisation efficiency, which could be due to its better adsorptive capacity. The characteristic peak of MB observed at 595 nm[30] shifted towards a lower wavelength due to the change in the

pH of the dye solution. No new peaks emerged as a consequence of MB dye removal using CS, CS-Fe and CS-Fe/Ni nanoparticles which indicated that the removal of MB occurred primarily through the adsorption process and even after degradation, the degraded products also adsorbed onto the prepared nanoparticles.

The dye removal mechanism of prepared nanoparticles and chitosan was through degradation catalysed by Fe^0 and adsorption caused by iron oxide shell and chitosan. The Fe^0 nanoparticles destroy the chromophoric conjugation of the dye molecule not only through direct electron transfer but also through the production of atomic hydrogen[29]. Ni on the surface of Fe^0 acted as a catalyst which facilitated atomic hydrogen production and enabled the electron transfer through the iron oxide shell. This stimulated the Fe/Ni nanoparticle for a greater dye removal efficiency[31]. In addition, oxidative removal also played an important role in dye removal when using iron-based nanoparticles. As a stabiliser, chitosan protects the iron nanoparticles and increases the interaction between Fe^0 and dye and shows a synergetic effect on the dye removal. In this study, CS-Fe/Ni nanoparticles showed a higher dye removal efficiency than the CS-Fe nanoparticles, consistent with the previous assumptions[15].

FTIR spectroscopy

The FTIR spectrum of CS, CS-Fe and CS-Fe/Ni nanoparticles is shown in figure 4.8. The FTIR measurements were carried out to determine the possible interactions between the metallic nanoparticle and chitosan. A broad overlapping band of OH stretching and N-H stretching of amine in chitosan was observed in the region centred at 3354 cm^{-1}. The absorption band at 2875 cm^{-1} is attributed to the C-H stretching vibrations. The absorption appeared at 1643 cm^{-1} corresponds to the C=O stretching of amide. The N-H bending vibration of the 1^0 amines was displayed by the absorption peak at 1539 cm^{-1}. The band at 1377 cm^{-1} corresponds to the bending vibrations of O-H and deformation of $-CH_3$ and $-CH_2$. The absorption peak observed at 1051 cm^{-1} could be due to the stretching vibrations of C-O in 1^0 alcohol/C-O-C/C-N of 1^0 amine. The peak at 893 cm^{-1} corresponds to the bending vibrations of =CH and $=CH_2$[15,16,32].

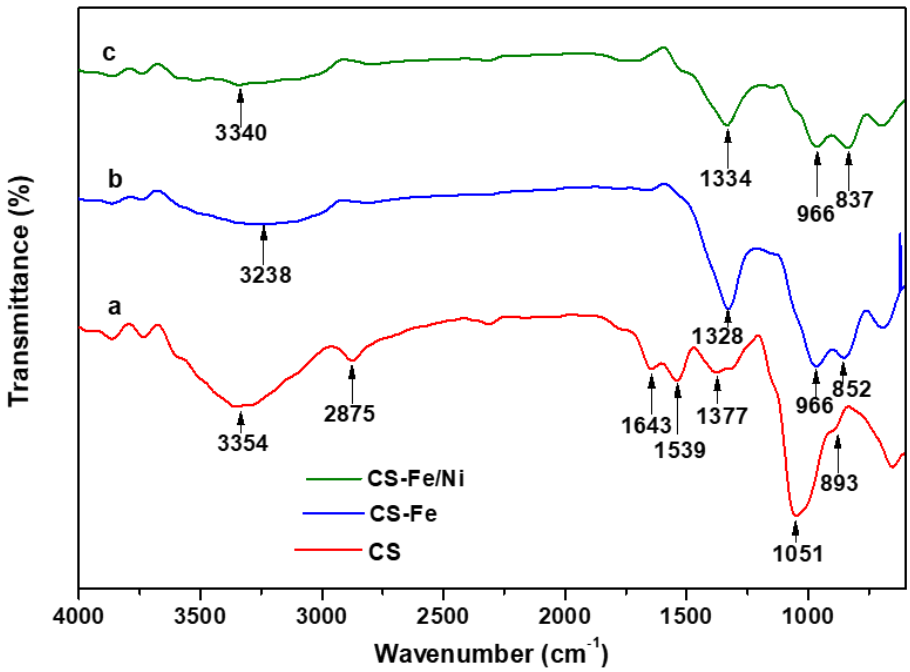

Figure 4.8 *FTIR spectra of (a) CS (b) CS-Fe and (c) CS-Fe/Ni nanoparticles*

The FTIR spectrum of CS-Fe and CS-Fe/Ni was different from that of the chitosan. The broad bands corresponding to O-H and N-H stretching of amine in chitosan was weakened and shifted to lower wavenumber in CS-Fe and CS-Fe/Ni. This may be due to the interaction of iron nanoparticles with these groups of chitosan. In addition to that, the intensity of peaks at 2875, 1643 and 1539 cm^{-1} decreased entirely and peaks at 1377, 1051 and 893 cm^{-1} shifted to lower wave number. From these results, it could be concluded that the iron interacted with amine and hydroxyl functional groups of chitosan, which proved to be a versatile stabiliser for zero valent iron. The addition of the second metal, Ni, possessed less significant changes in the FTIR spectra of CS-Fe/Ni compared with CS-Fe. This may be due to the low percentage of Ni in CS-Fe/Ni nanoparticles[15,32].

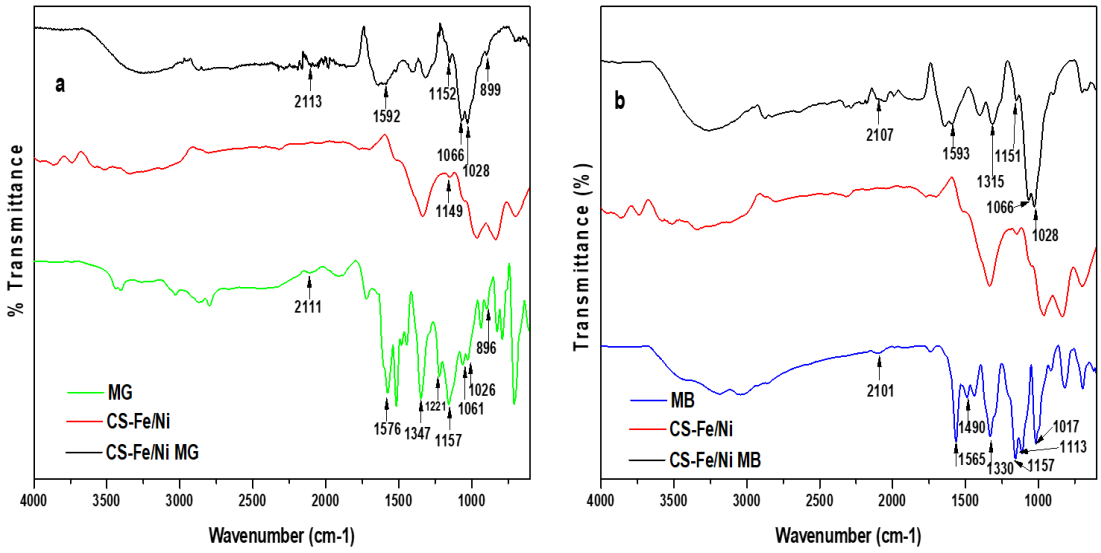

Figure 4.9 *FTIR spectra of CS-Fe/Ni nanoparticles after the removal of (a) MG and (b)MB*

FTIR spectra of CS, CS-Fe and CS-Fe/Ni nanoparticles showed remarkable changes after reacting with MB and MG dyes. The pattern of the fingerprint region changed due to the interaction between the prepared nanoparticles and dyes. Figure 4.9 (a,b) shows the FTIR spectra of CS-Fe/Ni nanoparticles after reacting with MG and MB dyes respectively. In the case of parent MG dye, the specific peaks in the fingerprint region (500-1500 cm^{-1}) match the mono-substituted and para-disubstituted benzene rings due to the C=C stretching of the benzene ring seen at 1576 cm^{-1}. MG also showed peaks at 1157 cm^{-1} and 1221 cm^{-1} corresponding to C-N stretching vibrations[33]. The peaks of parent MG dye are also seen in CS-Fe/Ni nanoparticles after reacting with MG. Some of the bands of MG get vanish, which indicates the destruction of the structure of MG in CS-Fe/Ni nanoparticles. The CS-Fe/Ni nanoparticles showed a similar peak of C=C stretching at 1592 cm^{-1}. The absence of peaks between 850–670 cm^{-1} supports the total disappearance of some aromatic rings of MG on reaction with the prepared nanoparticles. The peaks at 1221 cm^{-1} and 1347 cm^{-1} correspond to the C-N stretching whereas C-H bending was absent in the CS-Fe/Ni nanoparticles after the reaction[34].

In the case of parent MB, the peak at the 1565 cm^{-1} corresponds to N-H stretching vibration and the bands at 1113-1490 cm^{-1} belong to the framework vibration of benzene rings. The peak observed at 1017 cm^{-1} can be assigned to the S=O stretching vibrations[35]. FTIR spectra of CS-Fe/Ni nanoparticles after treating with MB showed similar peaks of parent MB dye, indicating that some of the MB molecules are adsorbed onto the CS-Fe/Ni

nanoparticles. The MB peaks seen in CS-Fe/Ni nanoparticles exhibited a shift to lower wave number with the absence of few peaks. This suggests the destruction of the methyl blue structure by CS-Fe/Ni nanoparticles.

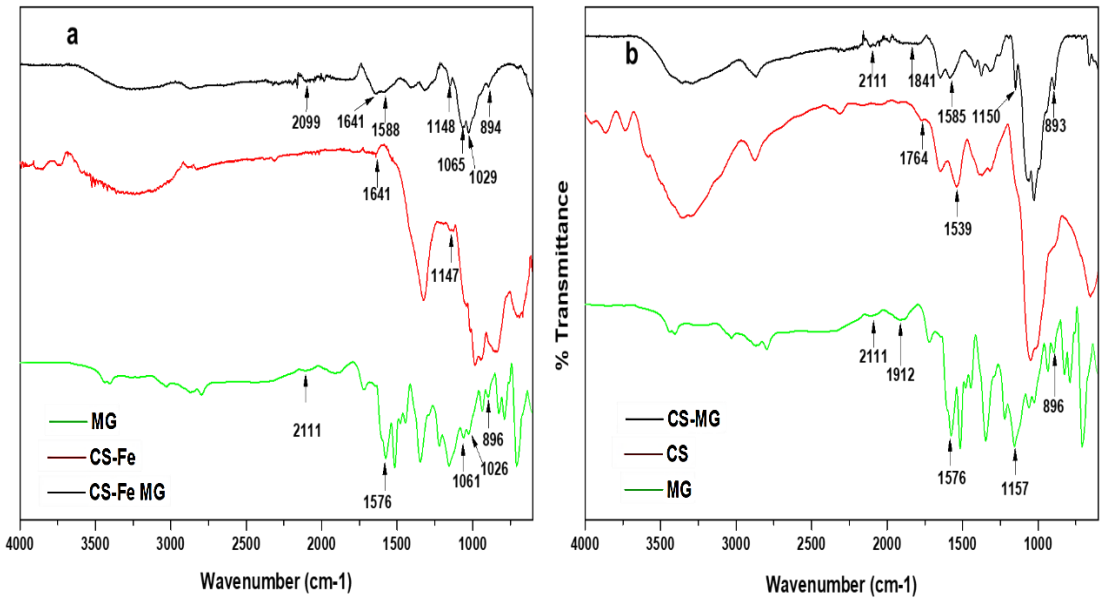

Figure 4.10 *FTIR spectra of CS-Fe (a) and CS (b) after treating with MG*

Figure 4.10 represents the FTIR spectra of CS-Fe (a) and CS (b) after MG dye removal and figure 4.11 corresponds to the FTIR spectra of CS-Fe (a) and CS (b) after MB dye removal. FTIR spectra of CS-Fe and CS nanoparticles after treating with MG/MB dyes showed a similar pattern of changes as CS-Fe/Ni nanoparticles. The spectra of CS, showed better similarity to parent MG/MB dye compared to that of CS-Fe and CS-Fe/Ni nanoparticles. This indicates that the removal of MG/MB by CS is mainly through adsorption.

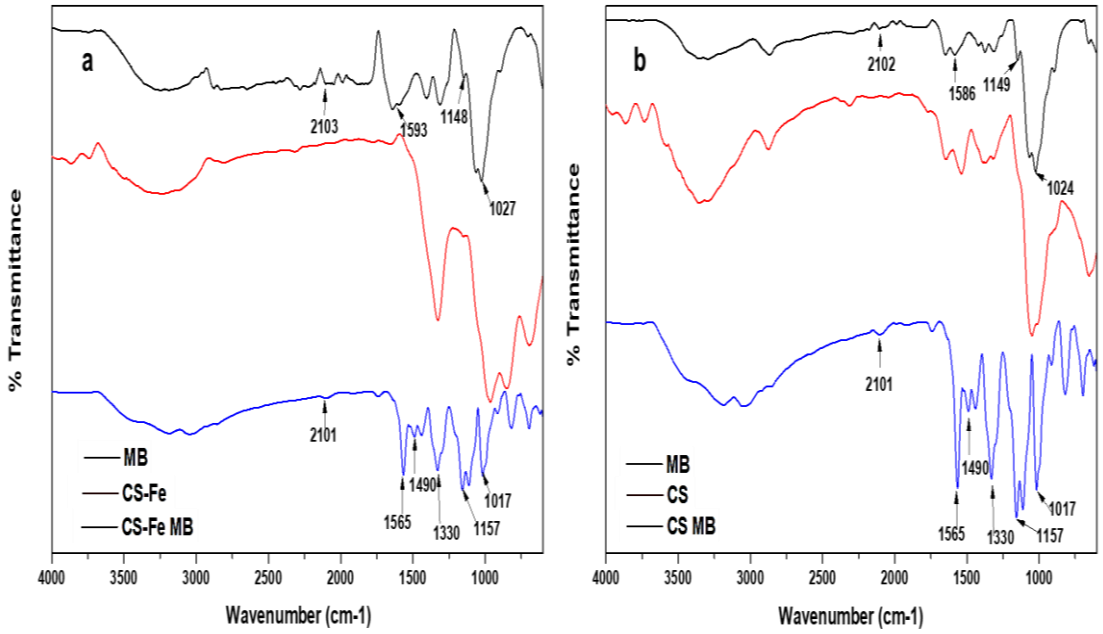

Figure 4.11 *FTIR spectra of CS-Fe (a) and CS (b) after treating with MB*

Effect of parameters on the removal of MG and MB

Effect of the initial concentration

The effect of the initial concentration of MG and MB dye was investigated in 20 mL of different dye concentrations ranging from 50 to 150 mg/L by using 2 g/L of CS, CS-Fe and CS-Fe/Ni nanoparticles, as shown in figure 4.12. The highest removal efficiencies of CS, CS-Fe and CS-Fe/Ni nanoparticles were 19 %, 88 % and 94 % respectively for MG and 74 %, 83 % and 85 % for MB at 50 mg/L of dye solution. The removal efficiencies seemed to be decreasing with an increase in the initial concentration of the dyes. The extensive percentage removal of MG by CS-Fe and CS-Fe/Ni is through a complex heterogeneous reaction greatly influenced by adsorptive and degradative pathways exhibited by Fe and chitosan. However, the removal of MB is primarily through the adsorption of prepared nanoparticles and chitosan. Degradation may take place on the adsorbed dye molecules. With the increase in dye concentration, the extent of adsorption also increases, but since the increase in dye molecules with concentration overwhelmed the percentage of dye molecules adsorbed, the overall effect is a decrease in dye removal efficiency with an increase in dye concentration.

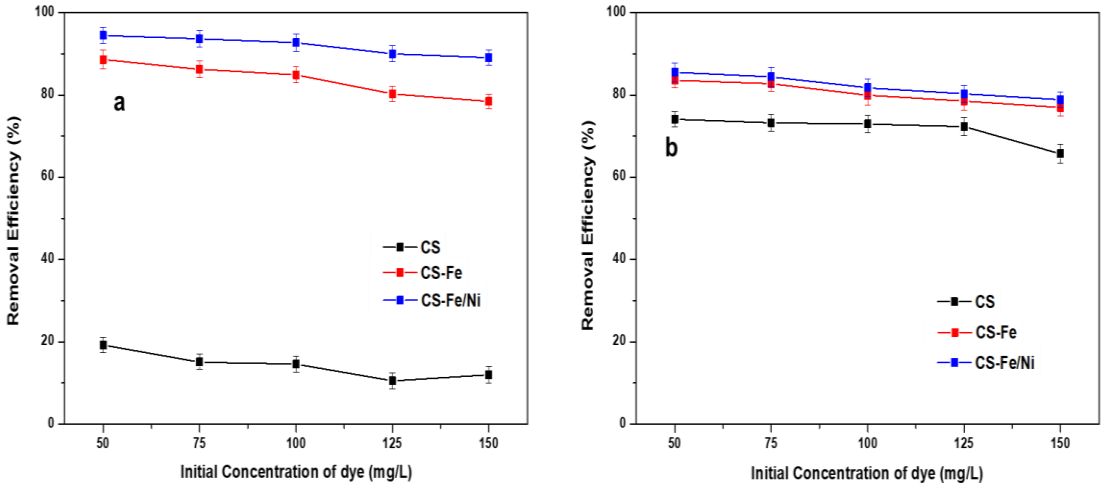

Figure 4.12 *Effect of initial dye concentration on dye removal (a) MG and (b) MB*

Effect of dosage of nanoparticles

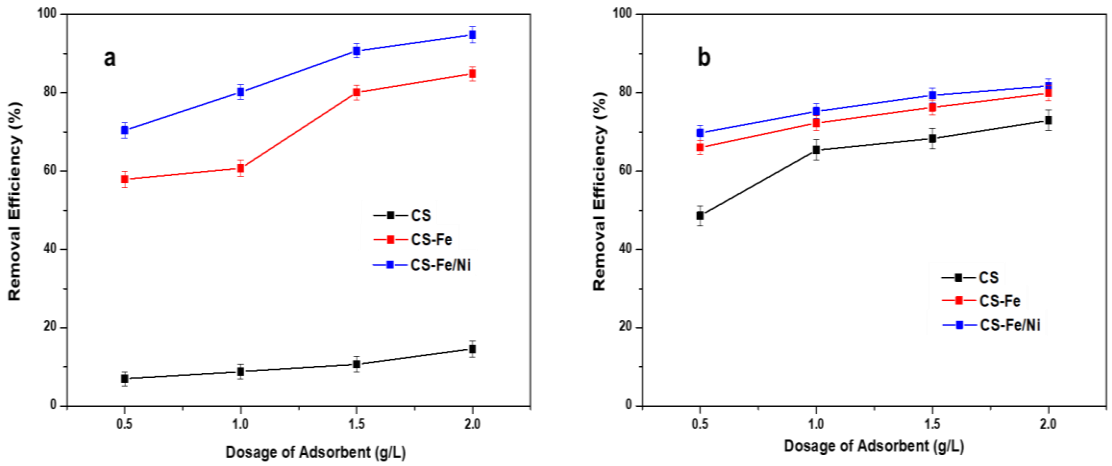

Figure 4.13 *Effect of dosage of nanoparticle in dye removal (a) MG and (b) MB*

The effect of nanoparticle dosage was studied in 4 different nanoparticle dosages, 0.5 g/L, 1 g/L, 1.5 g/L and 2 g/L of 50 mg/L of 40 mL dye solution as shown in figure 4.13. The highest removal efficiency, 94 % for MG and 82 % for MB, were seen in CS-Fe/Ni at 2 g/L. These results highlighted that the increase in dosage of CS-Fe and CS-Fe/Ni nanoparticles boosted the removal efficiency of MG and MB to a large extent. This was similar to the previous studies of dye removal using iron nanoparticles[36]. In the case of MB, chitosan also showed a high removal efficiency due to the adsorptive property of chitosan as a cationic polymer[37]. It is a well-known fact that the dye removal efficiency was greatly influenced by the concentration of available active reactive sites of Fe[30]. The increase in dosage of CS-Fe and CS-Fe/Ni nanoparticles with a small particles size

would increase the total surface adsorptive sites available for dye degradation and adsorption, which eventually lead to a higher dye removal efficiency of MG and MB.

Effect of contact time

Figure 4.14 illustrates the effect of contact time on MG and MB dye removal at 50 mg/L of dye solution of 40 mL using 2 g/L of the nanoparticle. The removal efficiency of MG and MB dyes has been studied at 3 different time intervals of 60,120,180 minutes. 99 % and 88 % dye removal for MG and MB respectively were obtained by CS-Fe/Ni nanoparticles within 180 minutes. The results show that the first 60 minutes exhibit a greater removal efficiency for MG and MB dye in CS-Fe and CS-Fe/Ni nanoparticles. The chitosan showed 77 % dye removal for MB in 180 minutes. This may be primarily due to the presence of tremendous empty active sites on the surface of Fe and chitosan. As the dye molecules were adsorbed onto the Fe surface and chitosan, the availability of active adsorptive sites decreased gradually leading to decrease in the removal efficiency rate in MG and MB dye with contact time.

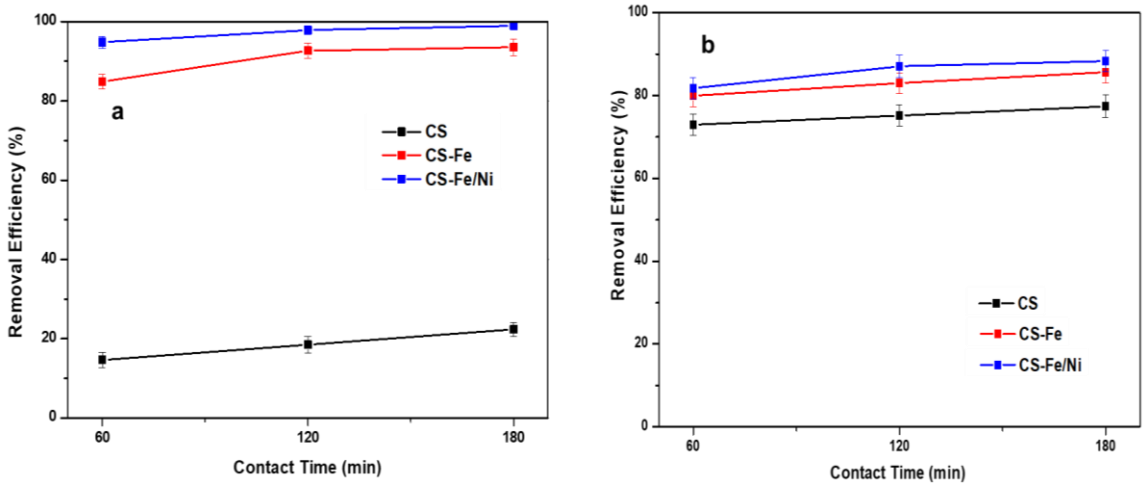

Figure 4.14 *Effect of contact time in (a) MG and (b) MB dye removal*

Effect of PH

The influence of pH on the MG and MB dye removal was studied at pH 4, pH 8 and pH 12 of 50 mg/L dye solution as shown in figure 4.15. The colour fading of triphenylmethane dyes with increased pH is due to the hydroxide ion attack on the central C atom of the planar ring system, thereby removing the conjugation[38]. The dye removal studies reveal that the highest removal efficiency for MG and MB occurred in acidic pH with 89 % dye removal for both MG and MB. The removal of MB and MG dye decreased with the

increase in pH of the solution. This is attributed to the hydroxide precipitation at the surface of iron nanoparticles at alkaline pH[39] which eventually leads to a decrease in the reactivity of CS-Fe and CS-Fe/Ni nanoparticles. From the above observations, it could also be concluded that simple adsorption takes place at higher pH. As the pH decreases, the depletion of the iron oxide shell and solubilisation of chitosan take place, exposing the inner Fe^0 core. Due to this, degradation takes place in addition to adsorption[40]. This leads to the more availability of iron nanoparticles for adsorption and degradation.

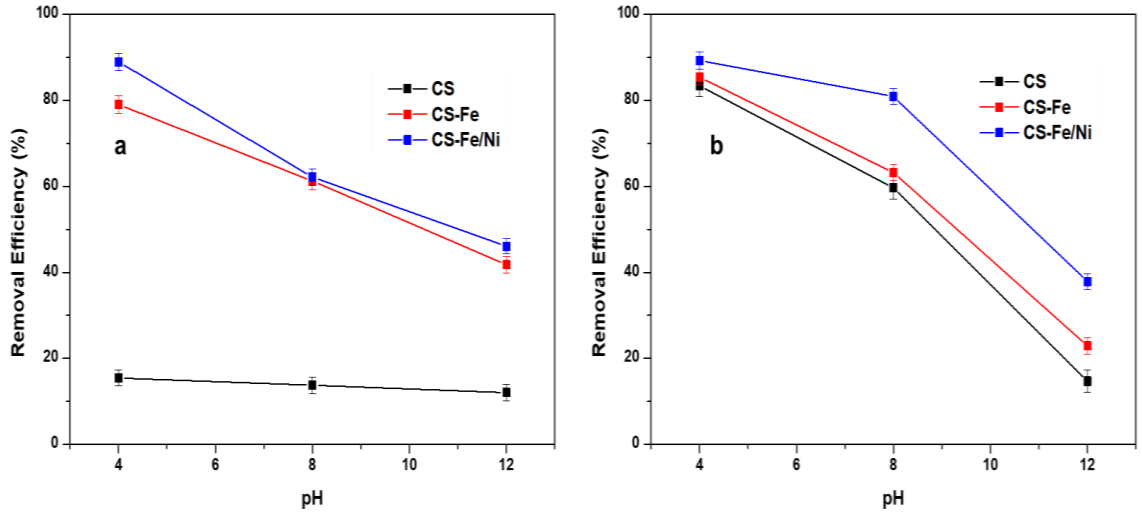

Figure 4.15 *Effect of pH in (a) MG and (b) MB dye removal*

Effect of Ionic Strength

The effect of ionic strength was studied by adding NaCl to the dye solution as shown in figure 4.16. The influence of ionic strength is studied in three different NaCl concentrations of 0.001 M, 0.01 M and 0.1 M. The introduction of the NaCl solution to the iron nanoparticles makes multiple effects on dye removal. When the NaCl concentration increases, the iron oxide shell drains away by reacting with the chloride ion. This will rejuvenate the Fe^0 surface and enhance dye degradation to a large extent. The results show that the introduction of NaCl has a negligible effect on MB adsorption with increasing ionic strength. These results indicate that the negatively charged Cl^- ions form a wall around the CS-Fe/Ni particles. Due to this, the methylene blue molecules cannot reach the nanoparticle surface, which eventually decreases its decolourisation[42]. In the case of MG, there is no significant decrease in dye removal with increasing ionic strength.

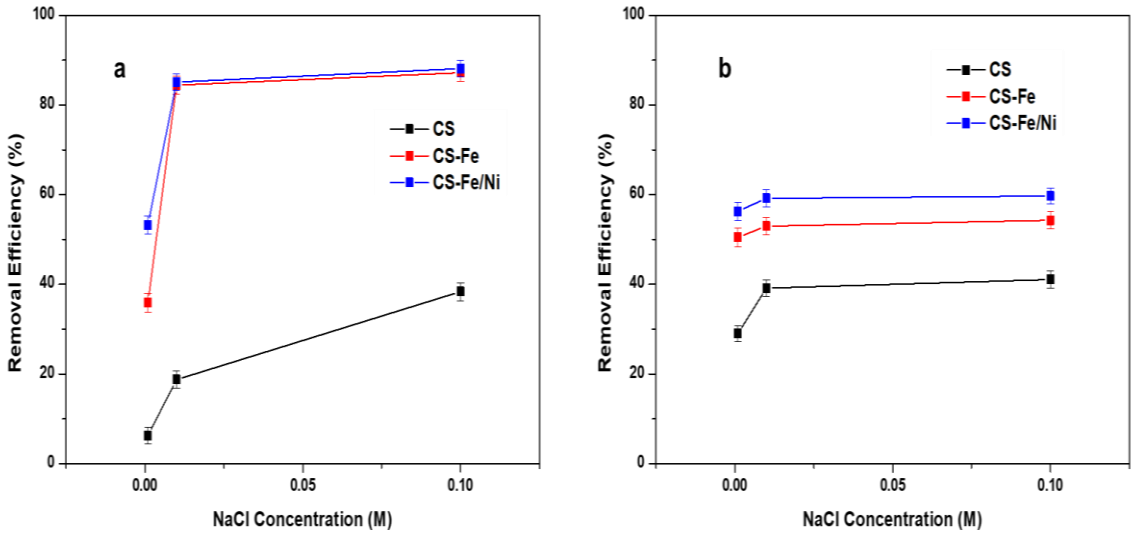

Figure 4.16 *Effect of ionic strength in (a) MG and (b) MB dye removal*

GC-MS/MS analysis

The GC-MS/MS analysis of MG dye after treating with CS-Fe/Ni nanoparticles has confirmed the degradation of MG dye molecules. GC-MS/MS analysis identified 4 degradation products such as (a) cyclohexa-2,5-diene-1,4-dione (MW 108), (b) diphenyl methanone (MW 182), (c) 4-nitrophenol (MW 139) and (d) 4-dimethylaminodiphenyl methane (MW 211) using the NIST library. Among the 4 identified degradation products, 4-nitrophenol and 4-dimethylaminodiphenylmethane were not detected in MG/Fe^0 system (chapter 3). The mass spectra of newly identified degradation products 4-nitrophenol (Rt 11.92) and 4-dimethylaminodiphenylmethane (Rt 22.91) are shown in figure 4.17(a & b) respectively. As displayed in scheme 4.1, the formation of 4-nitrophenol (a2) could result from the demethylation and OH addition reaction followed by oxidation of N,N-dimethylaniline (a) created during the degradation of MG dye molecules[45,46]. However, the formation of 4-dimethylaminodiphenylmethane (b2) could result from the hydrogenation of [4-(dimethylamino)phenyl]-phenylmethanone (b) in the presence of nickel as a catalyst since the deposition of CS-Fe with Ni improved the production of molecular hydrogen[47]. There were also some other chromatographic peaks in the spectrum which were not identified positively.

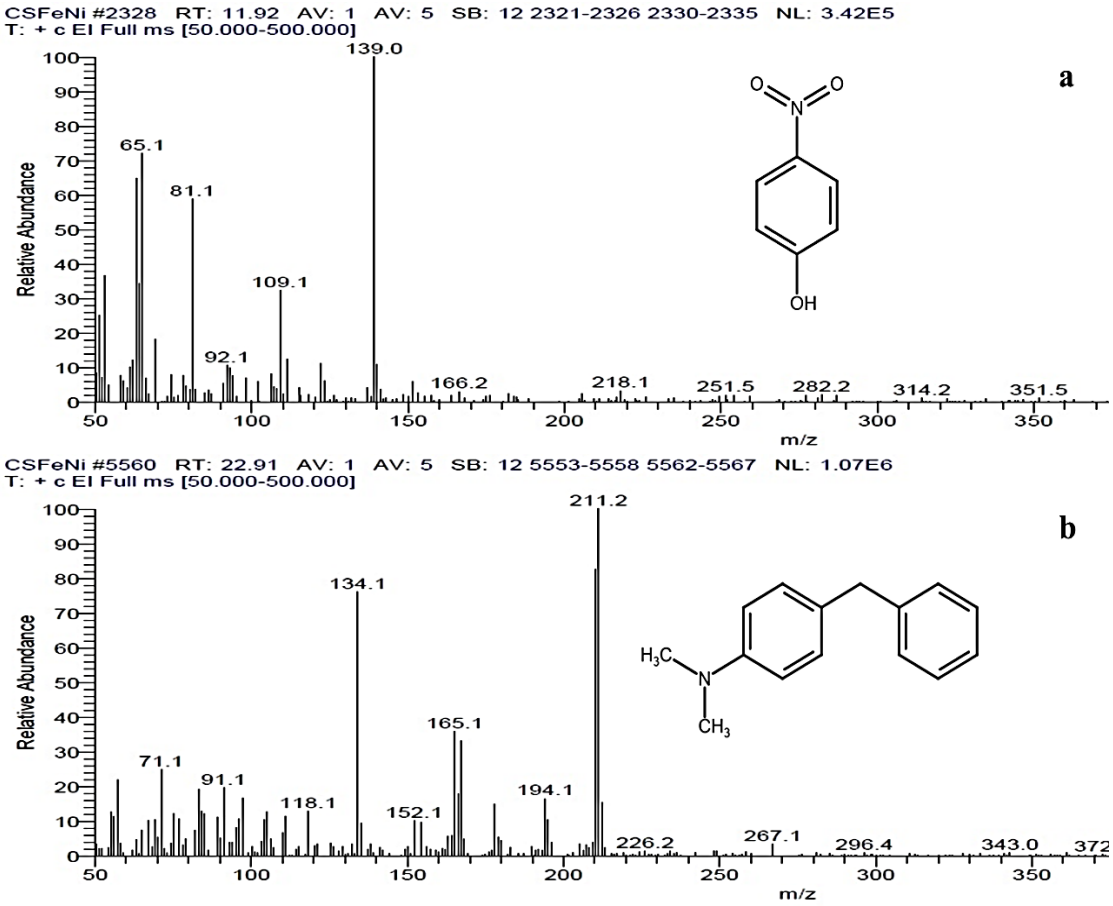

Figure 4.17 *Mass spectra of MG degradation products identified by GC-MS/MS analysis a) 4-nitrophenol and b) 4-dimethylaminodiphenylmethane.*

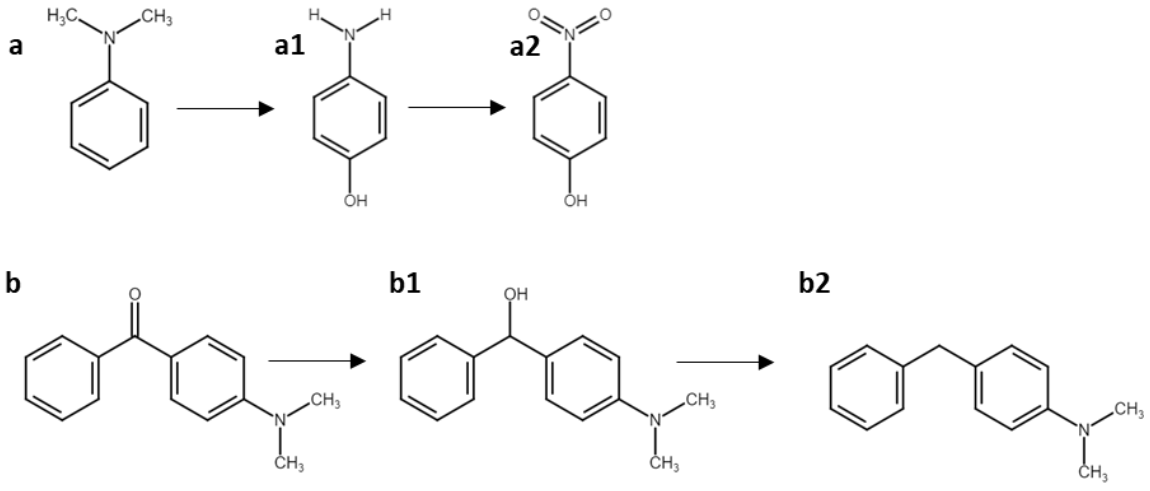

Scheme 4.1 *Degradation pathways of MG using CS-Fe/Ni nanoparticle*

4.4. Conclusions

The bimetallic Fe/Ni nanoparticles stabilised on the biopolymer chitosan (CS-Fe/Ni) established efficient Cr(VI) and dye removal compared with monometallic Fe stabilised on chitosan (CS-Fe) and the stabiliser chitosan (CS) alone. CS-Fe/Ni nanoparticles showed higher removal efficiency for hexavalent chromium. The cationic polymer, CS, also exhibited a high removal efficiency for anionic dye MB, which corresponded to the adsorptive property of the chitosan. The greater Cr(VI) and dye removal efficiency of CS-Fe/Ni nanoparticles were attributed to the small size of prepared nanoparticles and catalytic property of second metal Ni. The prepared nanoparticles displayed the effect of different parameters in the removal process of Cr(VI) and dye. The low pH of the solution was a favourable condition for the high pollutant removal efficiency of prepared nanoparticles. In general, the prepared CS-Fe/Ni nanoparticles were found more suitable for removing Cr(VI) and triphenylmethane dyes.

4.5. References

[1] T. Raychoudhury, T. Scheytt, Potential of Zerovalent iron nanoparticles for remediation of environmental organic contaminants in water: A review, Water Sci. Technol. 68 (2013) 1425–1439. https://doi.org/10.2166/wst.2013.358.

[2] B.D. Yirsaw, M. Megharaj, Z. Chen, R. Naidu, Environmental application and ecological significance of nano-zero valent iron, J. Environ. Sci. (China). 44 (2016) 88–98. https://doi.org/10.1016/j.jes.2015.07.016.

[3] W.J. Liu, T.T. Qian, H. Jiang, Bimetallic Fe nanoparticles: Recent advances in synthesis and application in catalytic elimination of environmental pollutants, Chem. Eng. J. 236 (2014) 448–463. https://doi.org/10.1016/j.cej.2013.10.062.

[4] G. Sharma, A. Kumar, S. Sharma, M. Naushad, R. Prakash Dwivedi, Z.A. ALOthman, G.T. Mola, Novel development of nanoparticles to bimetallic nanoparticles and their composites: A review, J. King Saud Univ. - Sci. 31 (2019) 257–269. https://doi.org/10.1016/j.jksus.2017.06.012.

[5] N. Ezzatahmadi, D.L. Marshall, K. Hou, G.A. Ayoko, G.J. Millar, Y. Xi, Simultaneous adsorption and degradation of 2,4-dichlorophenol on sepiolite-supported bimetallic Fe/Ni nanoparticles, J. Environ. Chem. Eng. 7 (2019) 102955. https://doi.org/10.1016/j.jece.2019.102955.

[6] S.L. Foster, K. Estoque, M. Voecks, N. Rentz, L.F. Greenlee, Removal of synthetic azo dye using bimetallic nickel-iron nanoparticles, J. Nanomater. 2019 (2019). https://doi.org/10.1155/2019/9807605.

[7] X. Weng, Z.Z. Chen, Z.Z. Chen, M. Megharaj, R. Naidu, Clay supported bimetallic Fe/Ni nanoparticles used for reductive degradation of amoxicillin in aqueous solution: Characterisation and kinetics, Colloids Surfaces A Physicochem. Eng. Asp. 443 (2014) 404–409. https://doi.org/10.1016/j.colsurfa.2013.11.047.

[8] Y. Gao, F. Wang, Y. Wu, R. Naidu, Z. Chen, Comparison of degradation mechanisms of microcystin-LR using nanoscale zero-valent iron (nZVI) and bimetallic Fe/Ni and Fe/Pd

nanoparticles, Chem. Eng. J. 285 (2016) 459–466. https://doi.org/10.1016/j.cej.2015.09.078.

[9] J. Adusei-Gyamfi, V. Acha, Carriers for nano zerovalent iron (nZVI): Synthesis, application and efficiency, RSC Adv. 6 (2016) 91025–91044. https://doi.org/10.1039/c6ra16657a.

[10] A. Pestov, S. Bratskaya, Chitosan and its derivatives as highly efficient polymer ligands, Molecules. 21 (2016). https://doi.org/10.3390/molecules21030330.

[11] S. Islam, M.A.R. Bhuiyan, M.N. Islam, Chitin and Chitosan: Structure, Properties and Applications in Biomedical Engineering, J. Polym. Environ. 25 (2017) 854–866. https://doi.org/10.1007/s10924-016-0865-5.

[12] H. Huang, Q. Yuan, X. Yang, Preparation and characterisation of metal-chitosan nanocomposites, Colloids Surfaces B Biointerfaces. 39 (2004) 31–37. https://doi.org/10.1016/j.colsurfb.2004.08.014.

[13] M. Ahmadi, M. Foladivanda, N. Jaafarzadeh, Z. Ramezani, B. Ramavandi, S. Jorfi, B. Kakavandi, Synthesis of chitosan zero-valent iron nanoparticles-supported for cadmium removal: Characterisation, optimisation and modeling approach, J. Water Supply Res. Technol. - AQUA. 66 (2017) 116–130. https://doi.org/10.2166/aqua.2017.027.

[14] A.A. Gonçalves, A.F. Araújo, M.J.M. Pires, R.M. Verly, D.V. Franco, L.M. Da Silva, Synthesis of chitosan-stabilised iron and nickel nanoparticles and the application in the reductive degradation of nimesulide, Eclet. Quim. 43 (2018) 10–25. https://doi.org/10.26850/1678-4618eqj.v43.1.10-25.

[15] X. Weng, S. Lin, Y. Zhong, Z. Chen, Chitosan stabilised bimetallic Fe/Ni nanoparticles used to remove mixed contaminants-amoxicillin and Cd (II) from aqueous solutions, Chem. Eng. J. 229 (2013) 27–34. https://doi.org/10.1016/j.cej.2013.05.096.

[16] B. Geng, Z. Jin, T. Li, X. Qi, Preparation of chitosan-stabilised Fe0 nanoparticles for removal of hexavalent chromium in water, Sci. Total Environ. 407 (2009) 4994–5000. https://doi.org/10.1016/j.scitotenv.2009.05.051.

[17] S.J. Gerber, E. Erasmus, Electronic effects of metal hexacyanoferrates: An XPS and FTIR study, Mater. Chem. Phys. 203 (2018) 73–81. https://doi.org/10.1016/j.matchemphys.2017.09.029.

[18] B. Desalegn, M. Megharaj, Z. Chen, R. Naidu, Green synthesis of zero valent iron nanoparticle using mango peel extract and surface characterisation using XPS and GC-MS, Heliyon. 5 (2019) e01750. https://doi.org/10.1016/j.heliyon.2019.e01750.

[19] Y. Momose, K. Tsuruya, T. Sakurai, K. Nakayama, Photoelectron emission and XPS studies of real iron surfaces subjected to scratching in air, water, and organic liquids, Surf. Interface Anal. 48 (2016) 202–211. https://doi.org/10.1002/sia.5942.

[20] Y. Xie, Y. Yi, Y. Qin, L. Wang, G. Liu, Y. Wu, Z. Diao, T. Zhou, M. Xu, Perchlorate degradation in aqueous solution using chitosan-stabilised zero-valent iron nanoparticles, Sep. Purif. Technol. 171 (2016) 164–173. https://doi.org/10.1016/j.seppur.2016.07.023.

[21] W. Huang, S. Ding, Y. Chen, W. Hao, X. Lai, J. Peng, J. Tu, Y. Cao, X. Li, 3D NiO hollow sphere/reduced graphene oxide composite for high-performance glucose biosensor, Sci. Rep. 7 (2017) 1–11. https://doi.org/10.1038/s41598-017-05528-1.

[22] G. Kurlyandskaya, L. Litvinova, A. Safronov, V. Schupletsova, I. Tyukova, O. Khaziakhmatova, G. Slepchenko, K. Yurova, E. Cherempey, N. Kulesh, R. Andrade, I. Beketov, I. Khlusov, Water-Based Suspensions of Iron Oxide Nanoparticles with Electrostatic or Steric Stabilisation by Chitosan: Fabrication, Characterisation and

Biocompatibility, Sensors. 17 (2017) 2605. https://doi.org/10.3390/s17112605.

[23] T. Liu, L. Zhao, D. Sun, X. Tan, Entrapment of nanoscale zero-valent iron in chitosan beads for hexavalent chromium removal from wastewater, J. Hazard. Mater. 184 (2010) 724–730. https://doi.org/10.1016/j.jhazmat.2010.08.099.

[24] P. Udaybhaskar, L. Iyengar, A.V.S.P. Rao, Hexavalent chromium interaction with chitosan, J. Appl. Polym. Sci. 39 (1990) 739–747. https://doi.org/10.1002/app.1990.070390322.

[25] C. Jiao, Y. Cheng, W. Fan, J. Li, Synthesis of agar-stabilised nanoscale zero-valent iron particles and removal study of hexavalent chromium, Int. J. Environ. Sci. Technol. 12 (2015) 1603–1612. https://doi.org/10.1007/s13762-014-0524-0.

[26] B. Kakavandi, R.R. Kalantary, M. Farzadkia, A.H. Mahvi, A. Esrafili, A. Azari, A.R. Yari, A.B. Javid, Enhanced chromium (VI) removal using activated carbon modified by zero valent iron and silver bimetallic nanoparticles, J. Environ. Heal. Sci. Eng. 12 (2014) 1–10. https://doi.org/10.1186/s40201-014-0115-5.

[27] S. Li, T. You, Y. Guo, S. Yao, S. Zang, M. Xiao, Z. Zhang, Y. Shen, High dispersions of nano zero valent iron supported on biochar by one-step carbothermal synthesis and its application in chromate removal, RSC Adv. 9 (2019) 12428–12435. https://doi.org/10.1039/c9ra00304e.

[28] M. Rivero-Huguet, W.D. Marshall, Reduction of hexavalent chromium mediated by micro- and nano-sized mixed metallic particles, J. Hazard. Mater. 169 (2009) 1081–1087. https://doi.org/10.1016/j.jhazmat.2009.04.062.

[29] Y. He, J.F. Gao, F.Q. Feng, C. Liu, Y.Z. Peng, S.Y. Wang, The comparative study on the rapid decolorisation of azo, anthraquinone and triphenylmethane dyes by zero-valent iron, Chem. Eng. J. 179 (2012) 8–18. https://doi.org/10.1016/j.cej.2011.05.107.

[30] X. Wang, P. Wang, J. Ma, H. Liu, P. Ning, Synthesis, characterisation, and reactivity of cellulose modified nano zero-valent iron for dye discoloration, Appl. Surf. Sci. 345 (2015) 57–66. https://doi.org/10.1016/j.apsusc.2015.03.131.

[31] A.D. Bokare, R.C. Chikate, C. V. Rode, K.M. Paknikar, Iron-nickel bimetallic nanoparticles for reductive degradation of azo dye Orange G in aqueous solution, Appl. Catal. B Environ. 79 (2008) 270–278. https://doi.org/10.1016/j.apcatb.2007.10.033.

[32] D. Jiang, D. Huang, C. Lai, P. Xu, G. Zeng, J. Wan, L. Tang, H. Dong, B. Huang, T. Hu, Difunctional chitosan-stabilized Fe/Cu bimetallic nanoparticles for removal of hexavalent chromium wastewater, Sci. Total Environ. 644 (2018) 1181–1189. https://doi.org/10.1016/j.scitotenv.2018.06.367.

[33] T. Bhagavathi Pushpa, J. Vijayaraghavan, S.J. Sardhar Basha, V. Sekaran, K. Vijayaraghavan, J. Jegan, Investigation on removal of malachite green using EM based compost as adsorbent, Ecotoxicol. Environ. Saf. 118 (2015) 177–182. https://doi.org/10.1016/j.ecoenv.2015.04.033.

[34] P. Raizada, P. Singh, A. Kumar, B. Pare, S.B. Jonnalagadda, Zero valent iron-brick grain nanocomposite for enhanced solar-Fenton removal of malachite green, Sep. Purif. Technol. 133 (2014) 429–437. https://doi.org/10.1016/j.seppur.2014.07.012.

[35] X. Yang, Z. Wang, M. Jing, R. Liu, F. Song, X. Shen, Magnetic nanocomposite Ba-ferrite/α-iron hollow microfiber: A multifunctional 1D space platform for dyes removal and microwave absorption, Ceram. Int. 40 (2014) 15585–15594. https://doi.org/10.1016/j.ceramint.2014.07.035.

[36] J. Guo, R. Wang, W.W. Tjiu, J. Pan, T. Liu, Synthesis of Fe nanoparticles@graphene composites for environmental applications, J. Hazard. Mater. 225–226 (2012) 63–73.

https://doi.org/10.1016/j.jhazmat.2012.04.065.

[37] S.-H. Lin, C.-P. Chang, J.-C. Chang, K. Mammel, Comparison of Dye Adsorption of Three Forms of Chitosan, Adv. Chem. Eng. Sci. 04 (2014) 319–326. https://doi.org/10.4236/aces.2014.43035.

[38] D.F. Latona, A.O. Dada, Kinetics of Reaction between Malachite Green and Hydroxyl Ion in the Presence of Reducing Sugars, J. Chem. Chem. Sci. 6 (2016) 1021–1028.

[39] L. Huang, F. Luo, Z. Chen, M. Megharaj, R. Naidu, Green synthesised conditions impacting on the reactivity of Fe NPs for the degradation of malachite green, Spectrochim. Acta - Part A Mol. Biomol. Spectrosc. 137 (2015) 154–159. https://doi.org/10.1016/j.saa.2014.08.116.

[40] F.S. Freyria, S. Esposito, M. Armandi, F. Deorsola, E. Garrone, B. Bonelli, Role of pH in the aqueous phase reactivity of zerovalent iron nanoparticles with acid orange 7, a model molecule of azo dyes, J. Nanomater. 2017 (2017). https://doi.org/10.1155/2017/2749575.

[41] T.S. Anirudhan, M. Ramachandran, Surfactant-modified bentonite as adsorbent for the removal of humic acid from wastewaters, Appl. Clay Sci. 35 (2007) 276–281. https://doi.org/10.1016/j.clay.2006.09.009.

[42] C. Sahoo, A.K. Gupta, Photocatalytic degradation of methyl blue by silver ion-doped titania: Identification of degradation products by GC-MS and IC analysis, J. Environ. Sci. Heal. - Part A Toxic/Hazardous Subst. Environ. Eng. 50 (2015) 1333–1341. https://doi.org/10.1080/10934529.2015.1059107.

[43] P. Yu, H. Yu, Q. Sun, B. Ma, Filter paper supported nZVI for continuous treatment of simulated dyeing wastewater, Sci. Rep. 9 (2019) 1–8. https://doi.org/10.1038/s41598-019-47863-5.

[44] N. Sleiman, V. Deluchat, M. Wazne, M. Mallet, A. Courtin-Nomade, V. Kazpard, M. Baudu, Phosphate removal from aqueous solutions using zero valent iron (ZVI): Influence of solution composition and ZVI aging, Colloids Surfaces A Physicochem. Eng. Asp. 514 (2017) 1–10. https://doi.org/10.1016/j.colsurfa.2016.11.014.

[45] C. Berberidou, I. Poulios, N.P. Xekoukoulotakis, D. Mantzavinos, Sonolytic, photocatalytic and sonophotocatalytic degradation of malachite green in aqueous solutions, Appl. Catal. B Environ. 74 (2007) 63–72. https://doi.org/10.1016/j.apcatb.2007.01.013.

[46] S. Singh, S.L. Lo, V.C. Srivastava, A.D. Hiwarkar, Comparative study of electrochemical oxidation for dye degradation: Parametric optimisation and mechanism identification, J. Environ. Chem. Eng. 4 (2016) 2911–2921. https://doi.org/10.1016/j.jece.2016.05.036.

[47] G. Bai, L. Niu, Z. Zhao, N. Li, F. Li, M. Qiu, F. He, G. Chen, Z. Ma, Ni–La–B amorphous alloys supported on SiO2 and γ-Al2O3 for selective hydrogenation of benzophenone, J. Mol. Catal. A Chem. 363–364 (2012) 411–416. https://doi.org/10.1016/j.molcata.2012.07.018.